CONDENSED MATTER PHYSICS

Multiple-*q* noncollinear magnetism in an itinerant hexagonal magnet

R. Takagi[1]*, J. S. White[2], S. Hayami[3], R. Arita[1,4], D. Honecker[5], H. M. Rønnow[6], Y. Tokura[1,4], S. Seki[1,7]*

Multiple-*q* spin order, i.e., a spin texture characterized by a multiple number of coexisting magnetic modulation vectors *q*, has recently attracted attention as a source of nontrivial magnetic topology and associated emergent phenomena. One typical example is the triple-*q* skyrmion lattice state stabilized by Dzyaloshinskii-Moriya interactions in noncentrosymmetric magnets, while the emergence of various multiple-*q* states of different origins is expected according to the latest theories. Here, we investigated the magnetic structure of the itinerant polar hexagonal magnet $Y_3Co_8Sn_4$, in which several distinctive mechanisms favoring multiple-*q* states are allowed to become active. Small-angle neutron-scattering experiments suggest the formation of incommensurate triple-*q* magnetic order with an in-plane vortex-like spin texture, which can be most consistently explained in terms of the novel four-spin interaction mechanism inherent to itinerant magnets. The present results suggest a new route to realizing exotic multiple-*q* orders and that itinerant hexagonal magnets, including the $R_3M_8Sn_4$ family with wide chemical tunability, can be a unique material platform to explore their rich phase diagrams.

INTRODUCTION

Recently, noncollinear and noncoplanar spin textures have been extensively investigated as a source of rich emergent phenomena. In particular, two- or three-dimensionally modulated multiple-*q* spin textures often display a nontrivial topology, which enables current-induced spin manipulation or magnetic control of electron transport properties through the emergent electromagnetic field associated with quantum Berry phase or relativistic spin-orbit interactions (*1*–*4*). For example, the triple-*q* state represented by the superposition of helical spin textures can be often considered as a crystallized form of magnetic skyrmions, i.e., noncoplanar swirling spin texture with topologically protected particle nature (*5*–*14*). Skyrmions are now attracting attention as information carriers and are providing a natural magnonic crystal potentially suitable for magnetic data processing (*15*–*18*), and the further search of exotic multiple-*q* states of novel origin is highly anticipated.

The formation of triple-*q* skyrmion states has been experimentally observed mainly in materials with noncentrosymmetric crystal structure, where the Dzyaloshinskii-Moriya (DM) interaction is the key for the emergence of helimagnetism (*16*, *17*). For these systems, the single-*q* helimagnetic order appears at zero magnetic field, and the application of a magnetic field stabilizes the hexagonal skyrmion lattice state with triple-*q* nature. Here, the detail of the spin texture depends on the symmetry of the crystal structure and associated DM interaction (*5*), and various forms of skyrmion spin textures, such as the Bloch-type one in the chiral system (*7*–*10*), the Néel-type one in the polar system (*11*–*13*), and the antivortex-type one in the D_{2d} symmetry system (*14*), have recently been discovered.

On the other hand, according to the latest theories, it is also expected that nontrivial multiple-*q* spin orders can be stabilized even without breaking of inversion symmetry. For example, magnetic frustration between the nearest neighboring and next nearest neighboring exchange interactions on the triangular lattice is proposed to stabilize the triple-*q* skyrmion order under the magnetic field applied along the out-of-plane direction (*19*–*21*). Another promising approach is the employment of itinerant magnetism in the high-symmetry (hexagonal or tetragonal) lattice system (*22*–*27*), where the four-spin interaction can stabilize various multiple-*q* orders even in zero magnetic field.

To realize the potential multiple-*q* helimagnetism expected from these novel mechanisms, the search for appropriate material systems fulfilling the corresponding conditions is essential. Our target material $Y_3Co_8Sn_4$ is a member of the $R_3M_8Sn_4$ (*R* being Y or a rare earth element and *M* being a 3*d* transition metal element) family characterized by a polar hexagonal crystal structure (Fig. 1A) and an itinerant nature of the magnetism (*28*–*30*). This material family is unique because all of the abovementioned mechanisms, i.e., (i) DM interaction in noncentrosymmetric systems, (ii) frustrated exchange interactions in triangular lattice systems, and (iii) four-spin interaction in itinerant hexagonal systems, are allowed to become active in principle, depending on the relative magnitude of each interaction. For $Y_3Co_8Sn_4$, the emergence of incommensurate magnetism has previously been proposed by a powder neutron diffraction study (*30*), while detailed information on the magnetic structure and associated mechanisms are still lacking.

In this work, we investigated the detailed magnetic structure for the itinerant hexagonal magnet $Y_3Co_8Sn_4$, through polarized and unpolarized small-angle neutron scattering (SANS) experiments on a single-crystal specimen under various applied magnetic fields and temperatures. Our results suggest the formation of triple-*q* magnetic order describing in-plane vortex-like spin textures, which can be most consistently explained in terms of the four-spin interaction mechanism activated in the itinerant hexagonal systems.

RESULTS

Figure 1A indicates the crystal structure of $Y_3Co_8Sn_4$, which belongs to the polar hexagonal space group $P6_3mc$ with the polar axis along the [001] direction (*25*). $Y_3Co_8Sn_4$ undergoes a ferromagnetic transition around 55 K (Fig. 1C, inset). The comparison of *M*-*H* (magnetization-magnetic field) profiles for $H \parallel [001]$ and $[1\bar{1}0]$ in Fig. 1B demonstrates

[1]RIKEN Center for Emergent Matter Science (CEMS), Wako 351-0198, Japan. [2]Laboratory for Neutron Scattering and Imaging (LNS), Paul Scherrer Institute (PSI), CH-5232 Villigen, Switzerland. [3]Department of Physics, Hokkaido University, Sapporo 060-0810, Japan. [4]Department of Applied Physics, The University of Tokyo, Tokyo 113-8656, Japan. [5]Institut Laue-Langevin, 71 avenue des Martyrs, CS 20156, F-38042 Grenoble Cedex 9, France. [6]Laboratory for Quantum Magnetism (LQM), Institute of Physics, École Polytechnique Fédérale de Lausanne (EPFL), CH-1015 Lausanne, Switzerland. [7]PRESTO, Japan Science and Technology Agency (JST), Tokyo 102-0075, Japan.
*Corresponding author. Email: rina.takagi@riken.jp (R.T.); shinichiro.seki@riken.jp (S.S.)

that the system has an easy-plane anisotropy perpendicular to the [001] axis. The saturation magnetization M_s is 0.35 μ_B/Co at 2 K. These magnetic properties are in good agreement with previous reports on polycrystalline samples (*29*, *30*). The temperature (T) dependence of the magnetic susceptibility (Fig. 1C) shows a notable reduction below 20 K, which implies a transition into the modulated spin state.

To elucidate the long-wavelength magnetic structure of $Y_3Co_8Sn_4$, we performed SANS measurements. Figure 1 (G to J) shows the temperature dependence of the SANS patterns measured on the (001) plane under zero magnetic field. At 1.5 K (Fig. 1G), we observe a sixfold symmetric pattern with magnetic Bragg reflections aligned along the $\langle 1\bar{1}0\rangle$ directions (equivalent to the a^* directions) and with a wave number of q_{out} ~0.081 A^{-1} that corresponds to a modulation period of 8 nm. In addition, we found a weak ring-shaped signal with a wave number of q_{in} ~ 0.040 A^{-1} (i.e., modulation period of 16 nm). On increasing the temperature, the sixfold q_{out} magnetic reflections become obscure around 14 K and vanish at T_1 = 18 K, while the ring-shaped q_{in} signal becomes stronger above 14 K and survives up to T_2 = 26 K. Figure 1D shows the temperature variations of the integrated intensities for q_{out} and q_{in}, taken for the boxed regions shown in Fig. 1J. The intensity due to sixfold q_{out} reflections is dominant below 13 K, while it is gradually replaced by the ring-shaped q_{in} intensity as the temperature increases. Above T_1 = 18 K, the ring-shaped q_{in} intensity becomes dominant, and then, it gradually disappears at T_2 = 26 K. Such a clear anticorrelation of intensity with temperature indicates that the two magnetic reflections q_{out} and q_{in} represent distinct magnetic phases and that their volume fractions vary with temperature. The distinctive nature of sixfold q_{out} and ring-shaped q_{in} can also be confirmed by the different temperature dependence of their wave numbers (Fig. 1E); the wave number of q_{out} monotonically decreases toward higher T, while that of q_{in} is almost temperature independent.

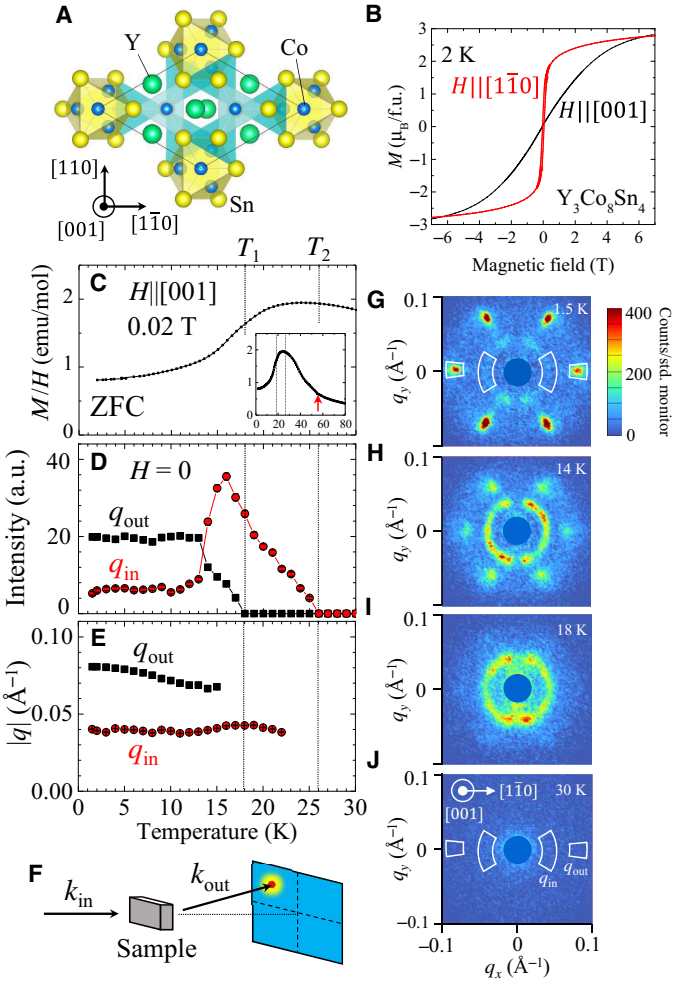

Fig. 1. Structural/magnetic properties and temperature dependence of SANS patterns for $Y_3Co_8Sn_4$. (**A**) Crystal structure of $Y_3Co_8Sn_4$. (**B**) Magnetic field dependence of the magnetization measured under H || [1$\bar{1}$0] (red) and H || [001] (black) at 2 K. (**C**) Temperature dependence of magnetic susceptibility (M/H at $\mu_0 H$ = 0.02 T) for H || [001]. (**D** and **E**) The integrated scattering intensity and the magnitude of the wave number for the two types of magnetic reflection, q_{out} and q_{in}, as a function of temperature obtained from SANS profiles. (**F**) Schematic illustration of the experimental geometry for SANS measurement. k_{in} and k_{out} are the incident and scattered neutron wave vectors, respectively. (**G** to **J**) SANS patterns measured for the (001) plane at zero magnetic field at various temperatures. The color scale indicates the scattering intensity. The integrated intensities in (D) are taken from the boxed area shown in (**J**). a.u., arbitrary units; f.u., formula unit.

Next, we investigate the magnetic field dependence of the magnetic scattering. Figure 2 (A to D and E to H) shows the SANS patterns at 1.5 K and in a magnetic field applied along the [001] and [1$\bar{1}$0] axes, respectively. For both q_{out} and q_{in}, the integrated intensities (Fig. 2, I and K) decrease monotonically with increasing H, accompanied by gradual increase of the wave numbers (Fig. 2, J and L). The SANS pattern described by q_{out} keeps the sixfold symmetry for both in-plane and out-of-plane orientations of H, even with a large H value close to the transition into the saturated ferromagnetic state. In contrast, the ring-shaped pattern of q_{in} is easily transformed into a twofold pattern under an in-plane H || [1$\bar{1}$0] (see fig. S1), which indicates the alignment of modulation vector q_{in} along the H direction.

To investigate the magnetic structures described by q_{out} and q_{in} in greater detail, we performed SANS with longitudinal neutron spin polarization analysis, using a ^{3}He spin analyzer setup, as shown in Fig. 3C. We used a longitudinal geometry, where the incident neutron spin polarization ($\boldsymbol{S}_n$) was aligned parallel to both the incident beam ($\boldsymbol{k}_{in}$) and the [001] axis of the sample. The longitudinal (parallel to $\boldsymbol{S}_n$) and transverse (perpendicular to $\boldsymbol{S}_n$) spin components of the magnetic order in the sample can be evaluated independently, since the corresponding magnetic scattering contributes to a purely non–spin-flipped (NSF) or spin-flipped (SF) response, respectively (Fig. 3D) (*31*). Thus, in our configuration, the SF (NSF) signal is due to spin components normal (parallel) to the [001] axis, which is referred to as S_{xy} (S_z). Figure 3 (A and B) shows polarized SANS patterns for the SF and NSF channels measured at 1.5 K under zero magnetic field. The magnetic reflections are observed in the SF channel but not in the NSF channel for both q_{out} and q_{in}. This proves that neither q_{out} nor q_{in} has a S_z component in the ground state, and therefore, the magnetic moments always lie within the (001) plane. The temperature development of each spin component for q_{out} and q_{in} is summarized in Fig. 3 (E and F). Note that the S_z component of q_{in} gradually becomes finite above 14 K, which may reflect the onset of spin fluctuations close to the critical temperature T_2.

On the basis of the present results, we have summarized the H-T phase diagrams for H || [001] and [1$\bar{1}$0] in Fig. 4 (A and B). Considering the observed alignment of modulation vectors along the in-plane H, the ring-shaped q_{in} pattern represents multiple domains of a single-q state with spin components modulating within the (001) plane, where the q vectors can orient randomly along any arbitrary in-plane direction (fig. S1). On the other hand, the observed SANS pattern of q_{out} maintains

a sixfold symmetry even under a large in-plane H, strongly suggestive of the formation of a triple-q spin texture.

The emergence of a unique multiple-q magnetic order has been predicted theoretically from various distinctive mechanisms, such as (i) DM interaction in noncentrosymmetric systems (*16*, *17*), (ii) frustrated exchange interactions in triangular lattice systems (*19*–*21*), and (iii) four-spin interaction in itinerant hexagonal systems (*26*, *27*). Since $Y_3Co_8Sn_4$ is characterized by a polar hexagonal crystal structure with itinerant magnetism, all of the above mechanisms may become active in principle. If the DM mechanism is responsible for the present case, then the polar symmetry of the crystal structure should favor cycloidal spin textures with magnetic moments confined within the *ac* plane, and application of $H \parallel [001]$ could lead to the formation of a triple-q Néel-type skyrmion lattice state (*5*, *11*–*13*, *32*). Both of these magnetic orders should contain nonzero magnitude of the S_z component. However, the observed confinement of the spins within the (001) plane is inconsistent with this scenario; therefore, the DM interaction is not the main source of incommensurate magnetism in $Y_3Co_8Sn_4$. Another potential source is frustrated exchange interactions, but this contribution is also determined to be minor because the Curie-Weiss temperature obtained from the temperature dependence of the inverse magnetic susceptibility is positive (i.e., ferromagnetic) and agrees well with T_c (*27*). Furthermore, this scheme rather assumes the frustration of short-ranged exchange interactions among localized moments, and its validity is less clear for the present case of $Y_3Co_8Sn_4$ with itinerant nature of magnetism. In principle, the two mechanisms above stabilize long-wavelength multiple-q spin orders only under an out-of-plane magnetic field. Therefore, the observed triple-q spin order at $H = 0$ in $Y_3Co_8Sn_4$ should be ascribed to a different origin.

On the basis of such an analysis, we focus on the mechanism associated with the four-spin interaction (*25*–*27*). In itinerant magnets, the Ruderman-Kittel-Kasuya-Yosida (RKKY) interaction usually favors the formation of a single-q helical spin order. On the other hand, from recent theoretical studies, it is suggested that multiple-q spin orders can be preferred because of additional four-spin interactions originating from electron hopping between four sites, when the system is characterized by a high-symmetry (i.e., hexagonal or tetragonal) crystal lattice (*25*–*27*). Since the magnetic anisotropy was not considered explicitly in previous theoretical works, we performed simulated annealing for the simple

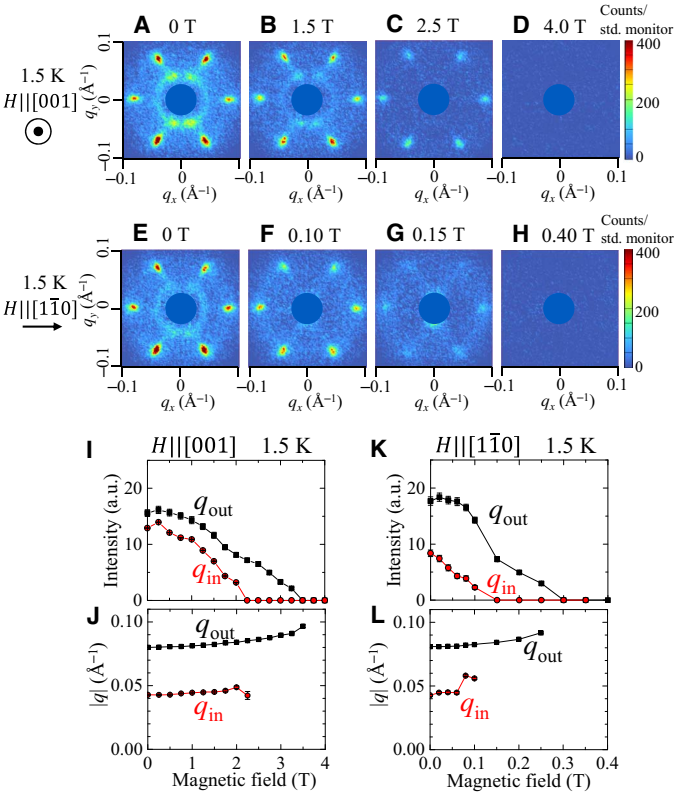

Fig. 2. Magnetic field dependence of SANS patterns for $Y_3Co_8Sn_4$. (**A** to **H**) SANS patterns taken at 1.5 K with various magnitudes of magnetic field for $H \parallel [001]$ (A to D) and $H \parallel [1\bar{1}0]$ (E to H). The color scale indicates the scattering intensity. (**I** to **L**) The scattering intensity and the magnitude of the wave number for two magnetic reflections q_{out} and q_{in} as a function of magnetic field, measured for $H \parallel [001]$ (**I** and **J**) and $H \parallel [1\bar{1}0]$ (**K** and **L**).

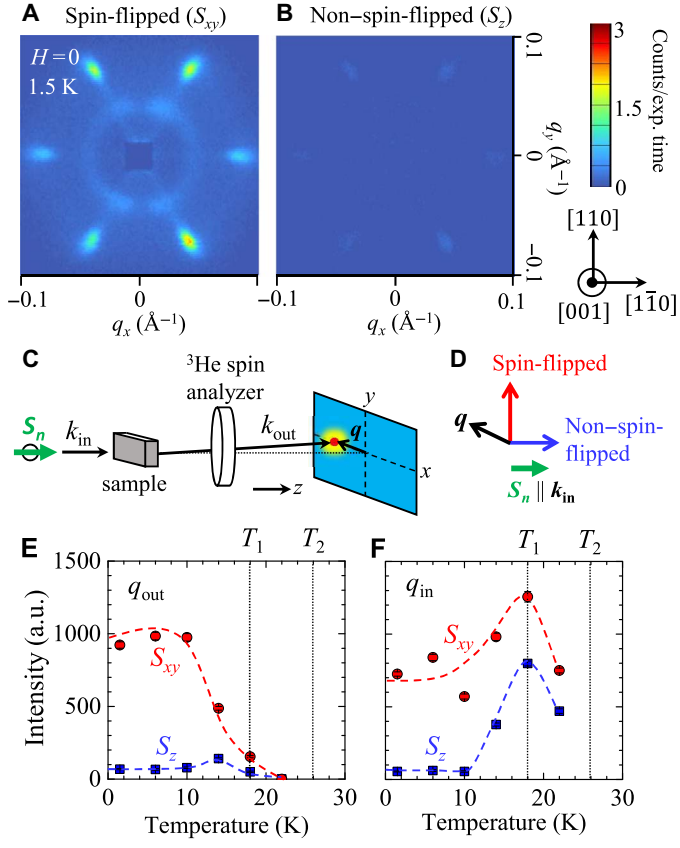

Fig. 3. Polarized SANS study of the modulated magnetic states at zero field. (**A** and **B**) Polarized SANS patterns of (A) SF and (B) NSF channels measured at 1.5 K under zero magnetic field, which detects in-plane and out-of-plane spin components (S_{xy} and S_z), respectively. The color represents the scattering intensity. (**C** and **D**) Schematic illustration of (C) experimental setup and (D) the magnetic scattering selection rules. Only a local magnetization normal to $\boldsymbol{q}$ can give rise to magnetic neutron scattering. The additional selection rules provided by the longitudinal polarized beam geometry are that SF scattering arises due to $\boldsymbol{S}_{xy}$ spin components perpendicular to both $\boldsymbol{q}$ and $\boldsymbol{k}_{in}$ (red arrow) and that NSF scattering arises due to $\boldsymbol{S}_z$ components $\parallel \boldsymbol{k}_{in}$ (blue arrow). Here, $\boldsymbol{S}_n$ represents the direction of the neutron polarization, which can be chosen experimentally to be either aligned or anti-aligned with $\boldsymbol{k}_{in}$. (**E** and **F**) Temperature variations of the scattering intensity of SF and NSF channels (corresponding to S_{xy} and S_z, respectively) for (E) q_{out} and (F) q_{in}. The data were integrated over the same detector regions, as shown in Fig. 1J.

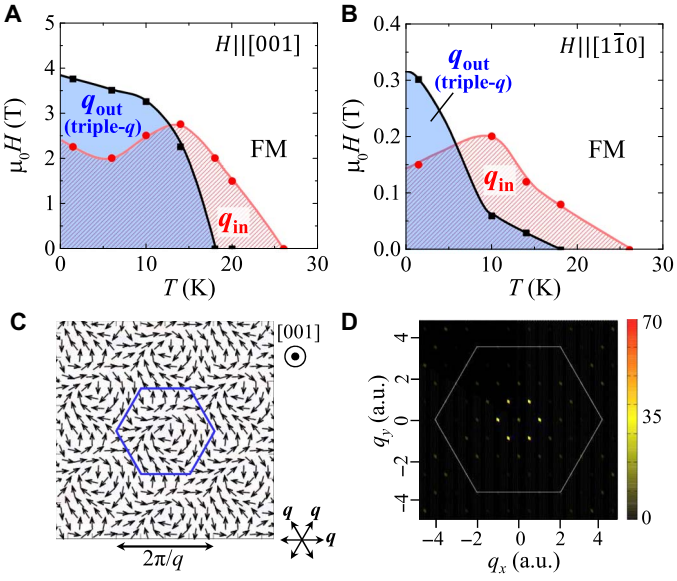

Fig. 4. Magnetic phases in $Y_3Co_8Sn_4$. (**A** and **B**) *H-T* magnetic phase diagrams derived from the field and the temperature dependence of the SANS intensity under (A) $H \parallel [001]$ and (B) $H \parallel [1\bar{1}0]$. (**C**) Triple-q spin configuration obtained by simulated annealing based on the model described by eq. S5, with the parameters $\alpha = 0.4$ and $K = 1.5$ ($\tilde{J} = 1$). Arrows represent the *xy* components of the magnetic moment. (**D**) Simulated SANS patterns corresponding to (C), with the color indicating the square root of the spin structure factor in arbitrary units. Hexagons in (C) and (D) represent the magnetic unit cell and first Brillouin zone, respectively.

hexagonal lattice system with additional easy-plane anisotropy based on the effective spin Hamiltonian proposed in (*27*) (see the Supplementary Materials for details). This result of the simulations confirms that the four-spin interaction can stabilize the vortex-like triple-q spin texture with moments confined within the hexagonal lattice basal plane, as shown in Fig. 4 (C and D), which is consistent with the present SANS results. Note that $Y_3Co_8Sn_4$ is characterized by a large crystallographic unit cell with four inequivalent Co sites, and the real spin texture in this compound may be more complicated due to the contribution of other factors neglected in the present model. For example, the observed appearance of a single-q order with a different modulation period at higher temperatures implies the delicate balance of competing instabilities associated with the intricate character of Fermi surfaces. Nevertheless, the main conclusion of this theoretical framework, i.e., the emergence of triple-q order with in-plane noncollinear spin textures in the ground state at $H = 0$, will be valid in general, irrespective of the material details.

DISCUSSION

The presently used four-spin interaction mechanism in itinerant magnets is unique, because it allows the emergence of multiple-q states even in zero magnetic field and without the necessity of inversion symmetry breaking. Recently, it has been reported that this four-spin interaction plays a key role in the emergence of a double-q square skyrmion lattice in the Fe monolayer on Ir(111), where the magnitude of the four-spin interaction turned out to be of the same order as the two-spin exchange interaction (*33*). Our present results for $Y_3Co_8Sn_4$ suggest that a similar mechanism may be also active in single-phase bulk itinerant magnets. Note that $Y_3Co_8Sn_4$ with easy-plane anisotropy is characterized by a coplanar spin texture, which is topologically trivial in terms of skyrmion number. On the other hand, the emergence of a noncoplanar multiple-q order with nonzero skyrmion number has theoretically been predicted for the system with weak or easy-axis magnetic anisotropy (*26*, *27*), and the systematic control of magnetic anisotropy is possible for the $R_3M_8Sn_4$ family due to its wide chemical tenability (*28*, *34*, *35*). Our experimental results suggest a new paradigm to realize exotic (and potentially topological) multiple-q orders and call for further exploration of other itinerant hexagonal magnets including the family of $R_3M_8Sn_4$.

MATERIALS AND METHODS

Sample preparation

Single crystals of $Y_3Co_8Sn_4$ were synthesized by arc-melting stoichiometric amounts of pure Y, Co, and Sn pieces, followed by slow cooling in a silica tube under vacuum. Powder x-ray diffraction analysis confirmed the single-phase nature of the crystal (fig. S4). The crystal orientation was determined by both x-ray Laue and neutron diffraction. The sample had a volume of 6 mm by 4 mm by 1 mm, with the widest surface parallel to the (001) plane.

Magnetization and SANS measurements

Magnetization was measured using a SQUID magnetometer (Magnetic Property Measurement System, Quantum Design). The SANS measurements were carried out using the SANS-I and SANS-II instruments at the Swiss Spallation Neutron Source (SINQ), Paul Scherrer Institut, Switzerland, and the D33 instrument at the Institut Laue-Langevin (ILL), Grenoble, France. The wavelengths of the neutron beam were set to 5 Å (SANS-I and SANS-II) and 4.6 Å (D33). The incident beam was always directed along the [001] axis. The SANS diffraction patterns were obtained by summing together two-dimensional multidetector measurements taken over a range of sample + cryomagnet rotation (rocking) angles. Background data at each rocking angle were obtained for $T = 60$ K well above T_c and subtracted from data obtained at low T to leave only the magnetic signal. All H (magnetic field) scans were performed in the H-increasing process after zero-field cooling (ZFC), and T (temperature) scans were performed in the warming process after ZFC.

In the SANS experiments, with longitudinal polarization analysis (POLARIS) using D33 at the ILL (*36*), the incident neutron beam was spin polarized using an Fe-Si transmission polarizer, with the spin polarization reversible by means of an radio frequency spin flipper. The neutron spin state after scattering from the sample was analyzed using a nuclear spin-polarized ^{3}He cell. The longitudinal neutron spin polarization axis was preserved by means of magnetic guide fields of the order of several milliteslas on the intermediate flight path between polarizer and analyzer. At the sample position, the guide field of 5 mT was applied by the cryomagnet, with the field being sufficiently low as the zero-field magnetic state of the sample was kept intact. The efficiency of the overall setup was characterized by the flipping ratio of 14. By measuring all possible spin-state combinations, corrections for the polarizing efficiency of the overall setup were taken into account in the data analysis. The polarized (and unpolarized) data reduction was performed using the GRASP software.

SUPPLEMENTARY MATERIALS

Supplementary material for this article is available at http://advances.sciencemag.org/cgi/content/full/4/11/eaau3402/DC1

Section S1. SANS investigation of q_{in} under in-plane magnetic field

REFERENCES AND NOTES

1. N. Nagaosa, Y. Tokura, Emergent electromagnetism in solids. *Phys. Scr.* **T146**, 014020 (2012).
2. A. Neubauer, C. Pfleiderer, B. Binz, A. Rosch, R. Ritz, P. G. Niklowitz, P. Böni, Topological Hall effect in the ***A*** phase of MnSi. *Phys. Rev. Lett.* **102**, 186602 (2009).
3. F. Jonietz, S. Mühlbauer, C. Pfleiderer, A. Neubauer, W. Münzer, A. Bauer, T. Adams, R. Georgii, P. Böni, R. A. Duine, K. Everschor, M. Garst, A. Rosch, Spin transfer torques in MnSi at ultralow current densities. *Science* **330**, 1648–1651 (2010).
4. T. Schulz, R. Ritz, A. Bauer, M. Halder, M. Wagner, C. Franz, C. Pfleiderer, K. Everschor, M. Garst, A. Rosch, Emergent electrodynamics of skyrmions in a chiral magnet. *Nat. Phys.* **8**, 301–304 (2012).
5. A. Bogdanov, A. Hubert, Thermodynamically stable magnetic vortex states in magnetic crystals. *J. Magn. Magn. Mater.* **138**, 255–269 (1994).
6. U. K. Rößler, A. N. Bogdanov, C. Pfleiderer, Spontaneous skyrmion ground states in magnetic metals. *Nature* **442**, 797–801 (2006).
7. S. Mühlbauer, B. Binz, F. Jonietz, C. Pfleiderer, A. Rosch, A. Neubauer, R. Georgii, P. Böni, Skyrmion lattice in a chiral magnet. *Science* **323**, 915–919 (2009).
8. X. Z. Yu, Y. Onose, N. Kanazawa, J. H. Park, J. H. Han, Y. Matsui, N. Nagaosa, Y. Tokura, Real-space observation of a two-dimensional skyrmion crystal. *Nature* **465**, 901–904 (2010).
9. S. Seki, X. Z. Yu, S. Ishiwata, Y. Tokura, Observation of skyrmions in a multiferroic material. *Science* **336**, 198–201 (2012).
10. Y. Tokunaga, X. Z. Yu, J. S. White, H. M. Rønnow, D. Morikawa, Y. Taguchi, Y. Tokura, A new class of chiral materials hosting magnetic skyrmions beyond room temperature. *Nat. Commun.* **6**, 7638–7644 (2015).
11. I. Kézsmárki, S. Bordács, P. Milde, E. Neuber, L. M. Eng, J. S. White, H. M. Rønnow, C. D. Dewhurst, M. Mochizuki, K. Yanai, H. Nakamura, D. Ehlers, V. Tsurkan, A. Loidl, Néel-type skyrmion lattice with confined orientation in the polar magnetic semiconductor GaV_4S_8. *Nat. Mater.* **14**, 1116–1122 (2015).
12. S. Bordács, A. Butykai, B. G. Szigeti, J. S. White, R. Cubitt, A. O. Leonov, S. Widmann, D. Ehlers, H.-A. Krug von Nidda, V. Tsurkan, A. Loidl, I. Kézsmárki, Equilibrium skyrmion lattice ground state in a polar easy-plane magnet. *Sci. Rep.* **7**, 7584 (2017).
13. T. Kurumaji, T. Nakajima, V. Ukleev, A. Feoktystov, T.-h. Arima, K. Kakurai, Y. Tokura, Néel-type skyrmion lattice in the tetragonal polar magnet $VOSe_2O_5$. *Phys. Rev. Lett.* **119**, 237201 (2017).
14. A. K. Nayak, V. Kumar, T. Ma, P. Werner, E. Pippel, R. Sahoo, F. Damay, U. K. Rößler, C. Felser, S. S. P. Parkin, Magnetic antiskyrmions above room temperature in tetragonal Heusler materials. *Nature* **548**, 561–566 (2017).
15. N. Romming, C. Hanneken, M. Menzel, J. E. Bickel, B. Wolter, Kirsten von Bergmann, A. Kubetzka, R. Wiesendanger, Writing and deleting single magnetic skyrmions. *Science* **341**, 636–639 (2013).
16. A. Fert, V. Cros, J. Sampaio, Skyrmions on the track. *Nat. Nanotechnol.* **8**, 152–156 (2013).
17. N. Nagaosa, Y. Tokura, Topological properties and dynamics of magnetic skyrmions. *Nat. Nanotechnol.* **8**, 899–911 (2013).
18. M. Garst, J. Waizner, D. Grundler, Collective spin excitations of helices and magnetic skyrmions: Review and perspectives of magnonics in non-centrosymmetric magnets. *J. Phys. D Appl. Phys.* **50**, 293002 (2017).
19. T. Okubo, S. Chung, H. Kawamura, Multiple-*q* states and the skyrmion lattice of the triangular-lattice Heisenberg antiferromagnet under magnetic fields. *Phys. Rev. Lett.* **108**, 017206 (2012).
20. A. O. Leonov, M. Mostovoy, Multiply periodic states and isolated skyrmions in an anisotropic frustrated magnet. *Nat. Commun.* **6**, 8275 (2015).
21. C. D. Batista, S.-Z. Lin, S. Hayami, Y. Kamiya, Frustration and chiral orderings in correlated electron systems. *Rep. Prog. Phys.* **79**, 084504 (2016).
22. I. Martin, C. D. Batista, Itinerant electron-driven chiral magnetic ordering and spontaneous quantum hall effect in triangular lattice models. *Phys. Rev. Lett.* **101**, 156402 (2008).
23. Y. Akagi, M. Udagawa, Y. Motome, Hidden multiple-spin interactions as an origin of spin scalar chiral order in frustrated Kondo lattice models. *Phys. Rev. Lett.* **108**, 096401 (2012).
24. D. Solenov, D. Mozyrsky, I. Martin, Chirality waves in two-dimensional magnets. *Phys. Rev. Lett.* **108**, 096403 (2012).
25. R. Ozawa, S. Hayami, K. Barros, G.-W. Chern, Y. Motome, C. D. Batista, Vortex crystals with chiral stripes in itinerant magnets. *J. Phys. Soc. Jpn.* **85**, 103703 (2016).
26. R. Ozawa, S. Hayami, Y. Motome, Zero-field skyrmions with a high topological number in itinerant magnets. *Phys. Rev. Lett.* **118**, 147205 (2017).
27. S. Hayami, R. Ozawa, Y. Motome, Effective bilinear-biquadratic model for noncoplanar ordering in itinerant magnets. *Phys. Rev. B* **95**, 224424 (2017).
28. F. Canepa, S. Cirafici, M. L. Fornasini, P. Manfrinetti, F. Merlo, A. Palenzona, M. Pani, Crystal structure of $R_3Co_8Sn_4$ compounds (R=Pr, Nd, Sm, Gd, Tb, Dy, Ho, Er, Tm, Yb, Lu, Y). *J. Alloys Compd.* **297**, 109–113 (2000).
29. F. Canepa, M. Napoletano, P. Manfrinetti, A. Palenzona, S. Cirafici, F. Merlo, Magnetic properties of $R_3Co_8Sn_4$ (R = Y, Gd). *J. Magn. Magn. Mater.* **220**, 39–44 (2000).
30. F. Canepa, M. Napoletano, A. Palenzona, O. Moze, W. Kockelmann, Ferromagnetic and incommensurate antiferromagnetic order in a multi-sublattice itinerant magnet: $Y_3Co_8Sn_4$. *J. Phys. Condens. Matter* **17**, 373 (2005).
31. R. M. Moon, T. Riste, W. C. Koehler, Polarization analysis of thermal-neutron scattering. *Phys. Rev.* **181**, 920 (1969).
32. R. Keesman, A. O. Leonov, P. van Dieten, S. Buhrandt, G. T. Barkema, L. Fritz, R. A. Duine, Degeneracies and fluctuations of Néel skyrmions in confined geometries. *Phys. Rev. B* **92**, 134405 (2015).
33. S. Heinze, K. von Bergmann, M. Menzel, J. Brede, A. Kubetzka, R. Wiesendanger, G. Bihlmayer, S. Blügel, Spontaneous atomic-scale magnetic skyrmion lattice in two dimensions. *Nat. Phys.* **7**, 713–718 (2011).
34. L. Gondeka, A. Szytulaa, S. Barana, A. Szajekb, J. Hernandez-Velasco, Neutron-diffraction studies of $R_3Co_8Sn_4$ (R=Y, Tb, Ho, Er) compounds. *Physica B* **350**, E123–E125 (2004).
35. V. V. Romaka, L. Romaka, I. Romaniv, E. K. Hlil, Z. Rykavets, B. Kuzhel, Crystallographic, magnetic and electrical characteristics of $R_3Ni_8Sn_4$ compounds (R = Y, Nd, Sm, Gd, and Tb). *J. Alloys Compd.* **701**, 358–365 (2017).
36. C. D. Dewhurst, I. Grillo, D. Honecker, M. Bonnaud, M. Jacques, C. Amrouni, A. Perillo-Marcone, G. Manzin, R. Cubitt, The small-angle neutron scattering instrument D33 at the Institut Laue-Langevin. *J. Appl. Crystallogr.* **49**, 1–14 (2016).
37. F. Izumi, K. Momma, Three-dimensional visualization in powder diffraction. *Solid State Phenom.* **130**, 15–20 (2007).
38. J. P. Perdew K. Burke, M. Ernzerhof, Generalized gradient approximation made simple. *Phys. Rev. Lett.* **77**, 3865–3868 (1996).
39. P. Blaha, K. Schwarz, G. K. H. Madsen, D. Kvasnicka, J. Luitz, R. Laskowski, F. Tran, L. D. Marks, WIEN2k software package; www.wien2k.at.

Acknowledgments: We thank O. Zaharko, K. Harada, K. Niitsu, D. Shindo, T. Matsumoto, D. Morikawa, X. Z. Yu, Y. Yamasaki, C. Tabata, H. Nakao, A. Kikkawa, Y. Motome, and T. Arima for helpful discussions and experimental support. This work is based on experiments performed at the Swiss Spallation Neutron Source SINQ, Paul Scherrer Institute, Villigen, Switzerland and the Institute Laue-Langevin, Grenoble, France. **Funding:** This work was supported by the Mitsubishi Foundation, by the JSPS Grants-In-Aid for Scientific Research (grant nos. 16H06590, 17H05186, and 18H03685), by JST PRESTO (grant no. JPMJPR18L5), by the Swiss National Science Foundation (SNF) Sinergia network "NanoSkyrmionics" (grant no. CRSII5-171003), by the SNF projects (grant nos. 153451 and 166298), and by the European Research Council project CONQUEST. **Author contributions:** S.S., H.M.R., and Y.T. conceived the project. R.T. contributed to the sample preparation and magnetization measurement. R.T., J.S.W., and D.H. performed SANS measurements. S.H. developed the theory. R.A. performed first-principles band structure calculation. The results were discussed and interpreted by all the authors. **Competing interests:** The authors declare that they have no competing interests. **Data and materials availability:** All data needed to evaluate the conclusions in the paper are present in the paper and/or the Supplementary Materials. Additional data related to this paper may be requested from the authors.

Submitted 31 May 2018
Accepted 19 October 2018
Published 16 November 2018
10.1126/sciadv.aau3402

Citation: R. Takagi, J. S. White, S. Hayami, R. Arita, D. Honecker, H. M. Rønnow, Y. Tokura, S. Seki, Multiple-*q* noncollinear magnetism in an itinerant hexagonal magnet. *Sci. Adv.* **4**, eaau3402 (2018).

Science Advances

Multiple-*q* noncollinear magnetism in an itinerant hexagonal magnet

R. Takagi, J. S. White, S. Hayami, R. Arita, D. Honecker, H. M. Rønnow, Y. Tokura and S. Seki

Sci Adv **4** (11), eaau3402.
DOI: 10.1126/sciadv.aau3402